EFFECT OF AXIAL LOAD INTENSITY ON PLASTIC HINGE LENGTH AND DAMAGE PROGRESS FOR LARGE SCALE RC COLUMNS DURING AN EARTHQUAKE ATTACK

Hakim BECHTOULA[1], Susumu KONO[2], Fumio WATANABE[3]

[1] PhD candidate, Dept. of Architecture and Architectural systems, Kyoto University
(Sakyo-ku, Kyoto 606-8501, Japan)
[2] Associate Professor, Dept. of Architecture and Architectural systems, Kyoto University
(Sakyo-ku, Kyoto 606-8501, Japan)
[3] Professor, Dept. of Architecture and Architectural systems, Kyoto University
(Sakyo-ku, Kyoto 606-8501, Japan)

ABSTRACT

To assess the main parameters affecting the damage progress four large-scale specimens with 560x560 mm were tested. It was found that number of cycles had an effect on the envelope of load-displacement curves, but a small effect on the lateral load carrying capacity. Analytical results such as moment-curvature and shortening-curvature relations, obtained using a simple fiber model, matched well the experimental ones. Paulay et al empirical equation underestimated the equivalent plastic hinge length, for specimens under a large axial load. Using IDARC, a non-linear frame program, load-displacement relation was predicted and compared to the experimental one. Damage progress based on Park et al model was also assessed using the same program, which reflect with a good accuracy the observed damage.

Keywords: Cyclic loading, Reinforced concrete, Capacity, Fiber model, Plastic hinge, Damage.

1. INTRODUCTION

The most widely observed damage for RC frames structures after an earthquake, is the collapse of the bearing columns. This collapse is expressed by the concrete crushing and buckling of the longitudinal reinforcement, which yields to the lost of the vertical bearing capacity. Understanding the parameters that influence the damage progress during an earthquake is a primordial issue. Sixteen cantilever reinforced concrete columns constituted of eight large-scale and eight small-scale specimens were tested to investigate the failure mode, scale effect as well as the damage progress. Only the last four large-scale specimens from our testing program will be presented hereafter, the results of the other specimens can be found elsewhere [1] and [2]. The behavior of the plastic hinge region was predicted using a fiber model where the confinement effect is taken into account. Strain transfer between the shear reinforcement and the concrete crushing was also clarified. Using the nonlinear IDARC program [3], the damage progress was assessed using Park at al damage index [4].

2. EXPERIMENTAL PROGRAM

2.1. TEST SETUP

The testing program was constituted of four large scales 560x560 mm cross section reinforced concrete columns with 1200mm as a shear span. The specimens were loaded under different axial intensity and horizontal loading path. Figure 1 shows the identical specimens configuration as well as the loading apparatuses. The axial load was kept constant for specimen L1N6B and L2N6B, and was varied for the last two specimens, L2NVB and L2NVC, as a linear combination of the sum of the moments as shown in Figure 2. In order to assess the effect of number of cycles on the bearing capacity the last two specimens were loaded in a square path with 2 and 4 cycles for each prescribed rotation angle respectively. The loading history is shown in Figure 3 (a) and (b). Sixty displacement gauges were provided at the lower part of the specimen to monitor the shear and flexural deformations. Figure 3 (c) shows the placement of these displacement gauges. The material characteristics and test variables fixed for this experimental are summarized in Table 1.

Table 1: Test variables

Specimen designation	Material			Test variables		
	Concrete strength f'c (Mpa)	Longitudinal rebar (ratio) [Fy]	Shear rebar (ratio) [Fy]	Axial force (axial force level in $f'cD^2$)	Slope in moment-axial force relation (MN/MN.m)	Lateral loading directions
L1N6B	32.2	12-D25 1.94% 388MPa	D13@100 0.91% 524MPa	Constant (0.6)	0	Uni
L2N6B						
L2NVB				Varied (0-0.6)	6	Bi
L2NVC						

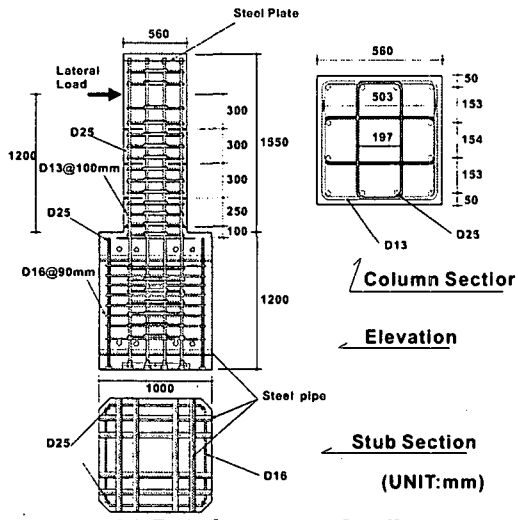

(a) Reinforcement details

Figure 1: Specimens configuration and loading system

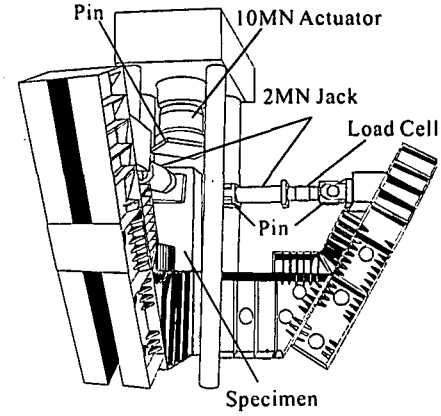

(b) Columns test setup

Figure 1: Specimens configuration and loading system

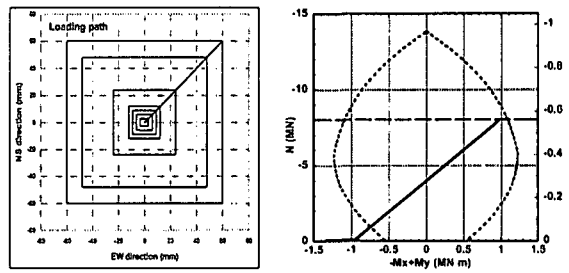

Figure 2: Top view of the loading path and the axial load variation

2.2. EXPERIMENTAL RESULTS

Since the shear failure was avoided during the design, all four specimens showed a ductile behavior until the test end. As seen in Figure 4, no big difference can be observed on the maximum lateral load between Specimens L2NVC and L2NVB. However, a large load drop can be seen for specimen L2NVC, from the 1st cycle to the 4th cycle at a rotation angle of 2% (24 mm). This effect can also be seen on the normalized moment-curvature curve in Figure 5. Besides the moment drop a considerable increase in curvature can be also observed. In Figure 6, normalized load versus the rotation angle envelope curves are shown for both specimens. The two envelope curves are lying on each other for a rotation angle less than 2%. Beyond that point a rapid drop is observed for specimen L2NVC due to the buckling of nearly all the longitudinal reinforcement bars. In the positive cycles of the NS direction, difference was observed at an early stage corresponding to 0.25% of rotation angle due to number of cycles under high axial load. Besides that, number of cycles had an effect on maximum sustained displacement as shown on the same figure.

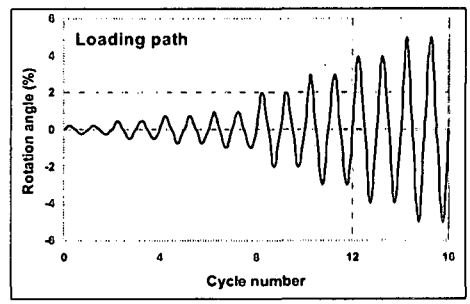

(a) L2NVB

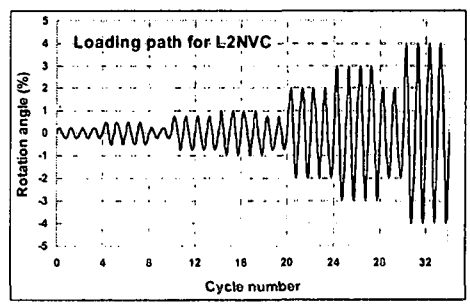

(b) L2NVC

Figure 3: Loading history and monitoring zone apparatus (Continue)

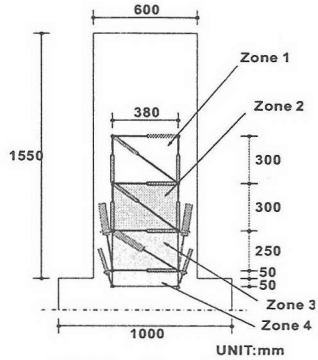

(c) Monitored zone

Figure 3: Loading history and monitoring zone apparatus

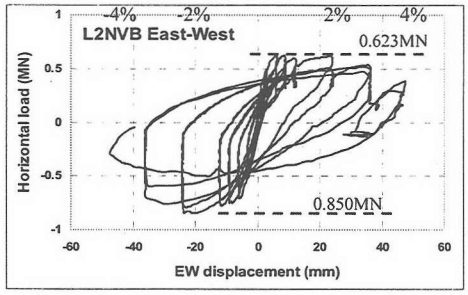

(a) L2NVB

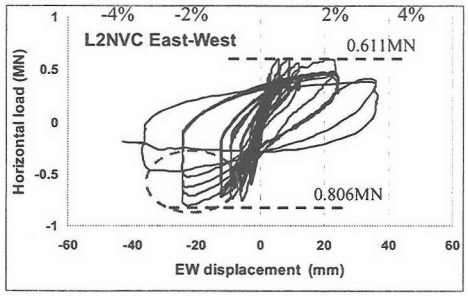

(b) L2NVC

Figure 4: Load-displacement relationship

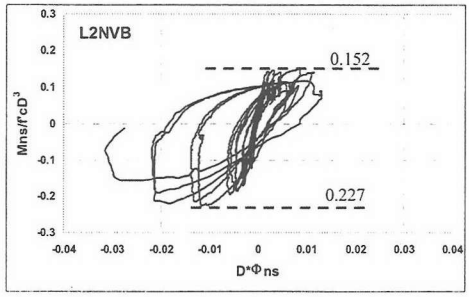

(a) L2NVB

Figure 5: Moment-curvature relationship (Continue)

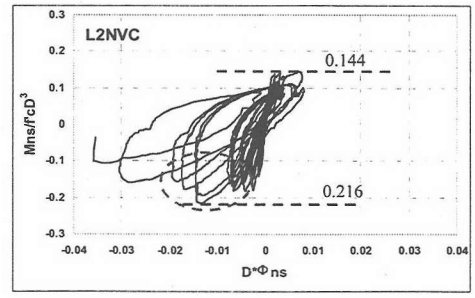

(b) L2NVC

Figure 5: Moment-curvature relationship

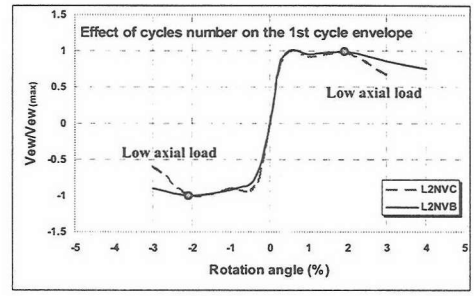

(a) EW direction

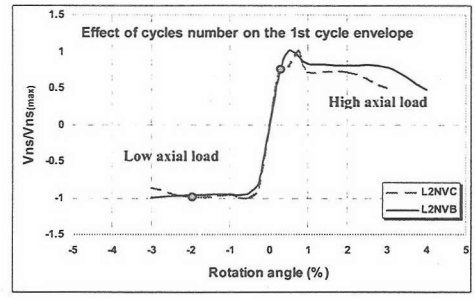

(b) NS direction

Figure 6: Load-displacement envelope curves

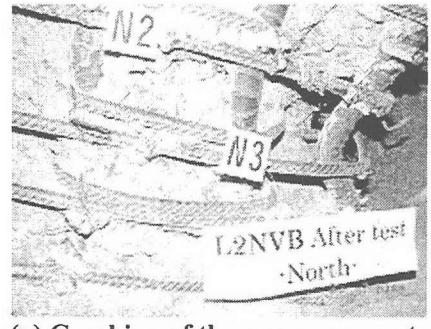

(a) Crushing of the corner concrete

Figure 7: Observed Damage (Continue)

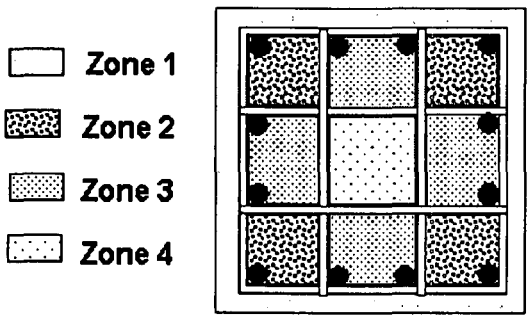

(b) Zoning of the observed damage progress

Figure 7: Observed Damage

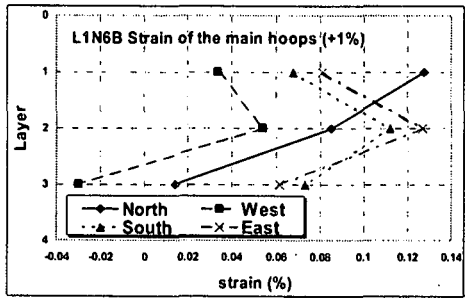

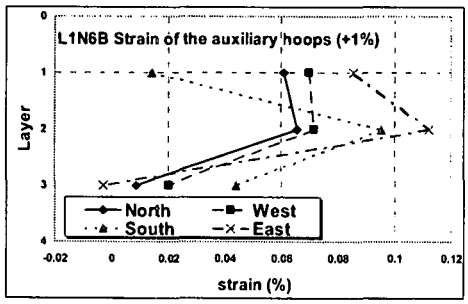

(a): At 1% rotation angle

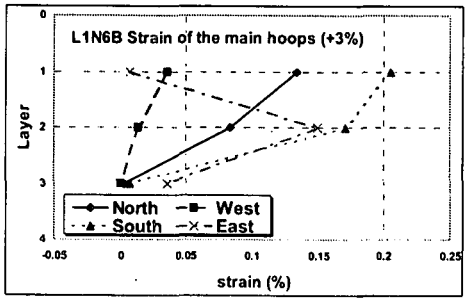

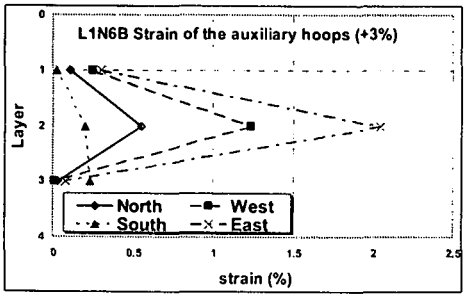

(b): At 3% rotation angle

Figure 8: Strain distribution for L1N6B specimen

During the test, concrete cover spalled first followed by buckling of longitudinal corner reinforcement. As test progressed, concrete at the corners started crushing as shown in Figure 7 (a), and gradually load carrying capacity started to reduce as damage penetrated toward the column core. This state can be seen through Figure 8, that shows the strain distribution of shear reinforcement at 1% and 3% rotation angles respectively. Strain of main shear reinforcement (exterior stirrups) started to reduce while an increase in strain of auxiliary shear reinforcement (internal stirrups) took place. This means that concrete at the peripheral of the core was severally damaged, hence effective concrete area reduced. Taking into account the observed damage and the results found using the shear reinforcement strain gauges, column section can be classified in 4 distinguished zones. These zones are shown in Figure 7 (b) and classified from1 to 4. Number attributed to the different zones indicates its crashing order.

3. ANALYTICAL RESULTS

The behavior of a plastic hinge was predicted using a simple fiber model. Section analysis was carried out assuming Bernoulli's theory for concrete and longitudinal steel. The column cross section was subdivide into concrete fiber elements and reinforcing steel fiber elements and the section response was obtained by integrating all fiber element stresses and stiffness. Steel fiber element followed the Ramberg-Osgood stress-strain relation, whereas concrete fiber element followed Popovic's stress-strain relation. The enhanced strength, f'_{cc}, due to confinement is expressed as follows.

$$f'_{cc} = f'_c + \kappa \rho_h f_{hy} \quad (1)$$

$$\kappa = 11.5\alpha\left(\frac{d}{C}\right)\left(1 - \frac{s}{2D_{core}}\right) \quad (2)$$

where f'_c is the cylinder compressive strength without confinement, κ, the coefficient of strength enhancement due to confinement, ρ_h, f_{hy}, d, and C the volume ratio, yield strength, diameter, and unsupported length of shear reinforcing bars, respectively, s the distance between adjacent shear reinforcement, and D_{core} the width of confined concrete. The coefficient, α, was added to the original equation by the authors to take into account the effects of strain gradient. Value of α was taken greater or equal to 1.0 to increase the strength and

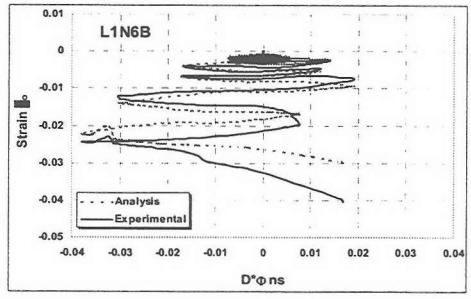

(a) L1N6B

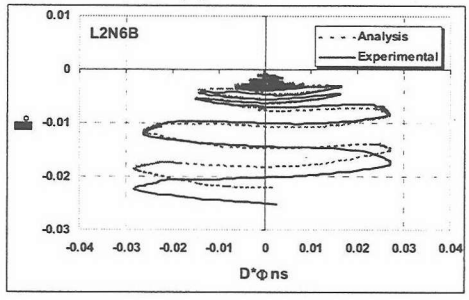

(b) L2N6B

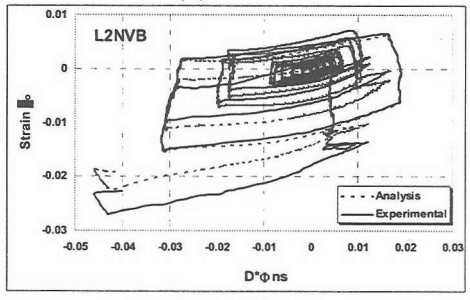

(c) L2NVB

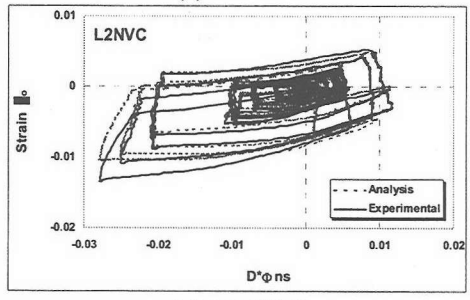

(d) L2NVC

Figure 9: Analytical and experimental axial strain results

ductility of confined concrete. The optimum values used in the analysis, are those giving the best fit between the prediction and the test results on the axial strain-normalized curvature curves. The obtained results are shown in Figure 9 for the four specimens, where a good agreement can be observed. Good agreement was also observed for the load-displacement curves that are not shown here due to space limitation.

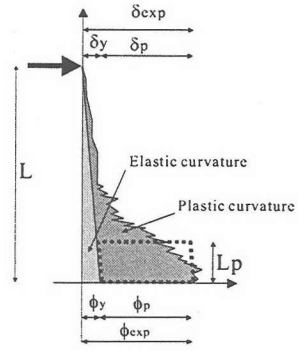

Figure 10: Parameters definition

4. EFFECT OF AXIAL LOAD INTENSITY ON THE EQUIVALENT PLASTIC HINGE LENGTH

$$\delta_p = \delta_{exp} - \delta_y = (L - L_p/2)\phi_p L_p$$
$$\phi_p = \phi_{exp} - \phi_y \quad (3)$$

$$L_p = 0.08(M/Q) + 0.022 d_b f_y \quad (4)$$

An equivalent plastic hinge length, EPHL, based on the experimental results was computed for all specimens using the proposed Equation (3). All parameters are defined in Figure 10. The EPHL were compared with those computed using Paulay and Priestley's empirical equation given in Equation (4).

It is clear from Figure 11 that Paulay and Priestly equation largely underestimated the EPHL for specimens under a high constant axial load, as shown in Figure 11(a). For specimens under a variable axial load, good results are observed for the sides under minimum axial load. However, for the sides under maximum axial load EPHL are underestimated, as shown in Figure 11(b). This difference can be explained using Figure 12, where curvature-rotation angle relationship is drawn for the monitored column base, zone 4 and 3 shown in the first part, Figure 3 (c). At maximum axial load side, zone 4 deformed in opposite direction than the rest of the column beyond 2% rotation angle point where buckling of longitudinal reinforcement was observed. This state is schematized in Figure 13. Even before the 2% rotation angle, the high axial load kept the curvature of the 4th zone very small compared to that in minimum axial load side, by consequence a large EPHL is required. These remarks are still valid for specimens L2N6B and L2NVC that are not shown in Figure 11.

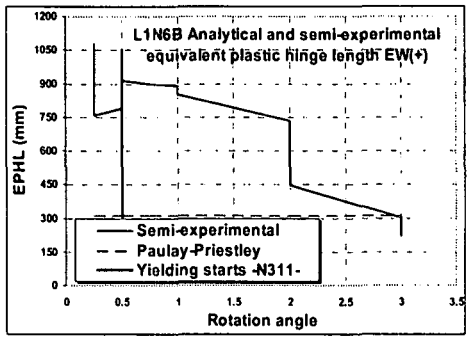

(a): L1N6B Constant axial load

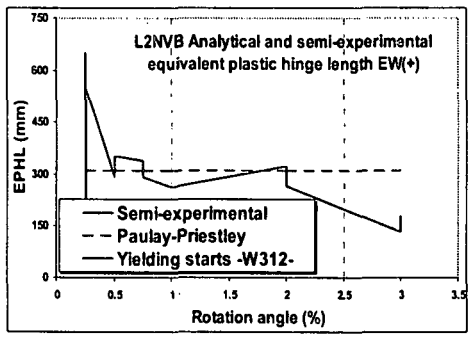

Low axial load

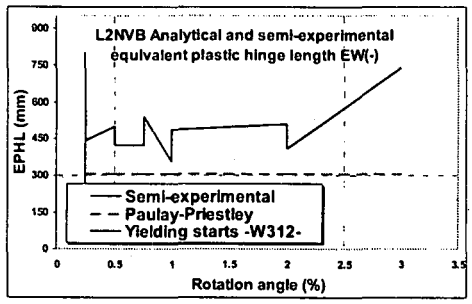

High axial load

(b): L2NVB Variable axial load

Figure 11:Equivalent plastic hinge length

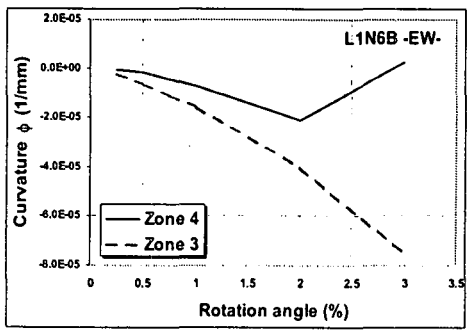

(a) L1N6B

Figure 12: Column base rotation (Continue)

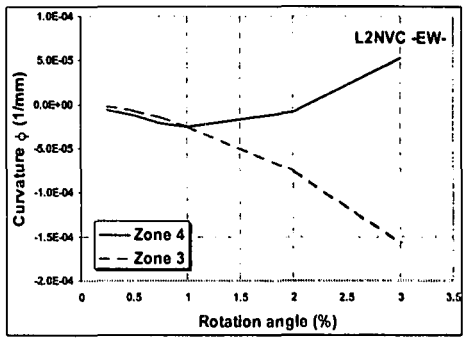

(b) L2NVC

Figure 12: Column base rotation

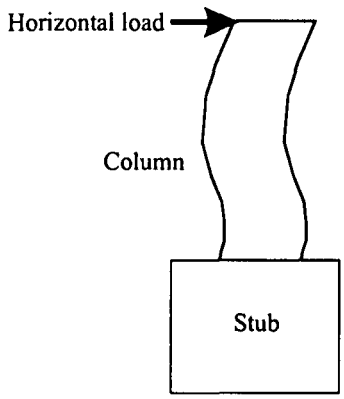

Figure 13: Deformed shape

5. DAMAGE EVOLUTION

The best known and most widely used of all cumulative damage indices is that of Park and Ang (1985). This consists of a simple linear combination of normalized deformation and energy absorption:

$$D = \frac{\delta_m}{\delta_u} + \beta_e \frac{\int dE}{F_y \delta_u} \qquad (5)$$

where: δ_m = maximum deformation under earthquake, δ_u = ultimate deformation under monotonic deformation. F_y = Calculated yield strength, dE = incremental absorbed hysteretic energy, and β_e = a positive parameters. Values of the damage index are such that $D \geq 1.0$ signifies complete collapse or total damage. The advantage of this model is its simplicity, and the fact that it has been calibrated against a significant amount of observed seismic damage. The damage is classified as follow:

Table 2: Control parameters

Parameter	Meaning	Value
α	Stiffness degradation	5
β_d	Strength degradation based on ductility	0.3
β_e	Strength degradation based on energy	0.3
γ	Pinching coefficient	1 (No slip)

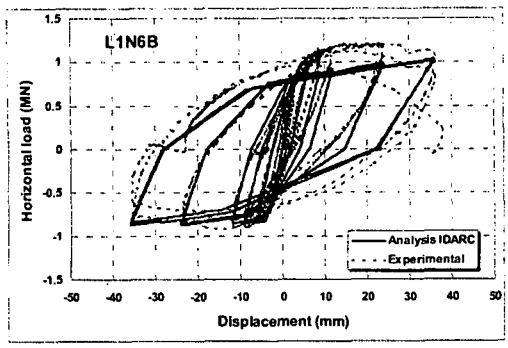

(a) Load-displacement

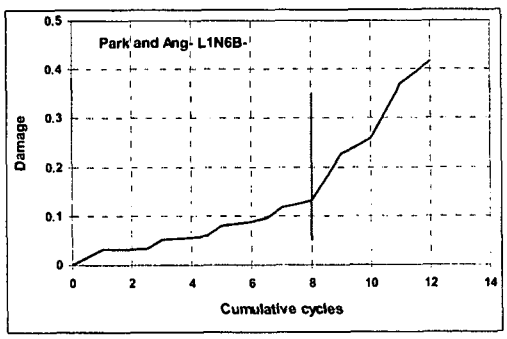

(b) Damage progress

Figure 14: Load-displacement and Damage progress assessed using IDARC program

- $D < 0.1$ No damage or localized minor cracking.
- $0.1 \le D < 0.25$ Minor damage- light cracking throughout.
- $0.25 \le D < 0.4$ Moderate damage- severe cracking, localized spalling.
- $0.4 \le D < 1.0$ Severe damage- crushing of concrete, reinforcement exposed.
- $D > 1.0$ Collapse.

More recently, Ang et al suggested using a value of $D = 0.8$ to represent collapse.

Using the more recent 2D version of IDARC program, the load displacement curve and the damage progress of specimen L1N6B were computed and shown in Figure 14. A good agreement for load-displacement is observed between the experimental and the analytical prediction using the control parameters shown in Table 2. It can also be seen on the same figure, that the damage rate increased more rapidly after the cycle number 8, which correspond to 2% rotation angle corresponding to excessive concrete crushing followed by the buckling of the longitudinal reinforcement, already discussed in section 2.2. At the end of the cyclic loading, the total damage was D=0.417, which corresponds, using the above classification, to "severe damage" range, which is more or less consistent with the observed one.

6. CONCLUSIONS

The following conclusions can be drawn from the test results and analytical study:

- Large drop in lateral load carrying capacity was observed for specimen loaded with 4 cycles (L2NVC) at 2% rotation angle. The corresponding curvature at 2% rotation angle increased rapidly from cycle 1 to cycle 4. The number of cycle had an effect on the envelope of load-displacement curves and sustained maximum displacement, but a small effect on the maximum lateral load or moment carrying capacities.
- A tied relation between concrete crushing progress and the strain transfer between external and internal hoops was found. Indeed, under a low rotation angle loading lateral concrete expansion was nearly equilibrated by the external hoops. However, while corner concrete started crushing, strain of peripheral hoops, started to reduce at the same time strain in the internal hoops started to increase. At this stage, mainly concrete enclosed by the internal hoops carried the axial load. In other words, increasing the number of internal shear reinforcement or changing the hoop configuration may improve considerably the confinement, and delay the strength degradation.
- Using a simple fiber model, the analytical results can match with enough precision the experimental ones by adjusting the new added coefficient to the original formulation, Eq. 1 and 2, that take into account the concrete strength enhancement.
- Paulay and Priestley's empirical equation underestimated the equivalent plastic hinge length for specimens under high axial load. For specimens under a variable axial load, good agreement was found only for the side under

minimum axial load. The cause was found to be the lower part of the column, which deformed in opposite direction to the rest of the column beyond 2% rotation angle. Curvature in maximum axial load side was kept very small compared to the side under minimum axial load; as a consequence a large equivalent plastic hinge length was required.

- The inelastic program IDARC successfully predicted the horizontal loading capacity for specimen L1N6B. Park and Ang damage index incorporated in IDARC program, was found to reflect with a good agreement the observed damage for the above mentioned specimen.

ACKNOWLEDGEMENT

The authors are thankful to M. Ando, M. Sakashita and Y. Arai, students at Kyoto University for their help during the test. Sincere thanks are extended to Prof. T. Kaku at Toyohashi University of Technology who gave us continues support and suggestions through the experimental. The authors also acknowledge TOPY Industries Limited, NETUREN Corporation Limited, and KOBE steel Limited for donating experimental materials.

REFERENCES

[1] Bechtoula, H., Arai, Y., Kono, S., Watanabe, F., "Damage Assessment of RC Columns Under Large Axial and Lateral Loadings" JCI symposium 2001, pp263-270 (in English).

[2] Kono, S., Bechtoula, H., Kaku, T., Watanabe, F., "Damage assessment of RC columns subjected to axial load and bi-directional bending" JCI journal 2002 PP235-240 (in Japanese).

[3] Valles, R., E., Reinhorn, A., M., Kunnath, S., K., Li, C., Madan, A., "IDARC2D Version 4.0: A computer program for the inelastic damage analysis of buildings" Technical report NCEER-96-0010 (in English).

[4] Young-Ji Park and Alfredo H.S. Ang "Mechanistic seismic damage model for reinforced concrete". Journal of structural engineering, ASCE, vol. 111, No. 4, April 1985, pp. 722-739 (in English).

[5] Paulay, T. and Priestley, M. N. J, "Seismic Design of Reinforced Concrete and Masonry Buildings ", New York: John Wiley & Sons 1992 (in English).